Climate Change and Ecological Engineering Jointly Induced Vegetation Greening in Global Karst Regions From 2001 to 2020

Jing Huang (jingjing520@email.swu.edu.cn)
Southwest University https://orcid.org/0000-0003-1378-6906
Zhongxi Ge
Southwest University, School of Geographical Sciences
Yuqing Huang
Nanning Normal University
Xuguang Tang
Southwest University, School of Geographical Sciences
Zhan Shi
Southwest University, School of Geographical Sciences
Peiyu Lai
Southwest University, School of Geographical Sciences
Zengjing Song
Southwest University, School of Geographical Sciences
Binfei Hao
Guangdong Ocean University
Hong Yang (h.yang4@reading.ac.uk)
Southwest University
Mingguo Ma
Southwest University, School of Geographical Sciences

Research Article

Keywords: Vegetation greenness trends, SINDVI, Climate factors, Human activities, Global karst regions

Posted Date: June 1st, 2021

DOI: https://doi.org/10.21203/rs.3.rs-192599/v1

REGULAR ARTICLE

Climate Change and Ecological Engineering Jointly Induced Vegetation Greening in Global Karst Regions From 2001 to 2020

Jing Huang[1, 2,3], Zhongxi Ge[1, 2,3], Yuqing Huang[5], Xuguang Tang[1, 2,3], Zhan Shi[1], Peiyu Lai[1,2,3], Zengjing Song[1,2,3], Binfei Hao[6], Hong Yang[2,4], Mingguo Ma[1, 2,3]

1 Southwest University, School of Geographical Sciences, Chongqing Jinfo Mountain Field Scientific Observation and Research Station for Karst Ecosystem, Ministry of Education, Chongqing 400715, China;

2 Chongqing Engineering Research Center for Remote Sensing Big Data Application, School of Geographical Sciences, Southwest University, Chongqing 400715, China;

3 Chongqing Key Laboratory of Karst Environment, School of Geographical Sciences, Southwest University, Chongqing 400715, China;

4 Department of Geography and Environmental Science, University of Reading, Whiteknights Reading, RG6 6AB, UK;

5 Key Laboratory of Beibu Gulf Environment Change and Resource Use, Ministry of Education ,Nanning Normal University, Nanning 530000, China;

6 College of Electronics and Information Engineering, Guangdong Ocean University, Zhanjiang 524088, China.

Corresponding author: Mingguo Ma; Hong Yang

Address: Tiansheng Road No.2, Beibei District, Chongqing 400715, China;

Whiteknights, RG6 6AB, Reading, Berkshire, United Kingdom

Tel: +86-23-6825-4917; 0044(0)1183787750

Fax: +86-23-6825-4917

Email：mmg@swu.edu.cn; h.yang4@reading.ac.uk

Abstract

Backgrounds Vegetation dynamic plays a dominant role in the global carbon cycle and climate, especially in vulnerable karst ecosystem. Many studies have examined past several decades changes in vegetation greenness and the associated with climate drivers. Yet, few studies have analyzed the vegetation change in global karst regions particularly in the last decades when climate change and anthropogenic disturbance widely occurred.

Methods In this study, we investigated the spatio-temporal variations of vegetation dynamic using the Seasonally Integrated Normalized Difference Vegetation Index (SINDVI) and examined their relationship to climate changes by correlation analysis, the ordinary least squares method investigate the variation trends and the Mann-Kendal test to detect the turning point from 2001 to 2020.

Results As expected, there have greening trend in global karst SINDVI from 2001 to 2020, with significant increasing trend in China (range = 0.836, $P < 0.05$), Europe (range = 0.456, $P < 0.05$) and many other regions. According to correlation analyses, SINDVI is water-limited in arid and semi-arid regions, such as Middle East and central Asia, and temperature-limited in northern high-latitude.

Conclusions consistent with previous studies, our results suggest that anthropogenic activities are mainly responsible for increasing vegetation greenness in tailoring management measures (e.g., Ecological Engineering, the Grain to Green Project) of China and Europe, intensive farmed in Middle East. Coupling warming temperature and increasing precipitation, southeastern Asia and Russia showed an increasing trend in SINDVI. In general, climate factors were the dominant drivers of the variation in vegetation greenness in globally karst regions during research period.

Keywords: Vegetation greenness trends · SINDVI · Climate factors · Human activities · Global karst regions

Introduction

Karst physiognomy is created by mechanical erosion and chemical solubility (Liu et al. 2012), and there are substantive movement and large reciprocity of water and rock in karst areas. The global area of karst regions is approximately 2.2×10^7 km^2, around 15% of global land areas (Falkowski et al. 2000). Karst dynamic system is characterized by the epikarst vegetation interaction, providing more than 25% of groundwater for global population (Cao et al. 2017). The karst ecosystem is particularly vulnerable mainly due to the alternation of seasonal drought and flood, soil erosion, surface subsidence, and rocky desertification (Huang et al. 2000; Yuan 1993). Under intensive anthropogenic disturbances and extreme climate changes, fragile karst terrains have been facing the threat of serious ecosystem degradation. This type of degradation often manifests as a reduction in vegetation cover and the consequence of soil erosion, is one of the most serious environmental problems in the world (Yuan 2000; Yue et al. 2010). Therefore, the dynamics of vegetation cover has been considered as an essential indicator of the ecosystem changes in karst regions (Kelly et al. 2011; Piao et al. 2015).

Vegetation is the main component of the terrestrial ecosystem and it plays an important role in global carbon cycle, water and energy balance. Under global climate change, how plant's photosynthesis responds to warming temperature and extreme climate events. Analysis vegetation greenness between temperature, precipitation are essential for designing policies to mitigate the passive impacts of extreme climate, anthropogenic activities on the well-being of mankind and environment (Begue et al. 2011, Peters et al. 2012). Chen et al. (2019); De Jong et al. (2013) have attempted to examined the causal factors responsible for the vegetation greenness by investi-

gating the response of vegetation to climate changes, as represented by variables such as temperature and precipitation. however, different geological backgrounds may result in significant differences in soil and moisture regimes for the weathered crust, which restricts the spatial allocation of regional water and soil, as well as constrains the geochemical cycling processes of nutrients, leading to impacts on vegetation greenness (Florinsky and Kuryakova 1996; Seddon et al. 2016). As for the driving factors for spatiotemporal changes in vegetation, natural elements such as elevation precipitation and air temperature are usually consider to explore the spatial distribution of greening or browning trends (Chen and Pan 2010; Jiang et al. 2017; Ndayisaba et al. 2016). Furthermore, anthropogenic effect also have a significant impact on vegetation dynamics and distribution (Martínez and Gilabert 2009). Many previous studies have investigated the relationship between human practices and vegetation variations at different spatial scales (Liu et al. 2018; Sun et al. 2015; Tong et al. 2017). The vegetation in karst regions is an essential part of the global ecosystem and has strong spatial heterogeneity in different regions (Cao et al. 2017; Vermote et al. 2002). Understanding the characteristics of temporal and spatial variation in vegetation cover, and quantitatively analyzing the correlation between its changes with geographical and climate factors, is critical to study the relationship of vegetation, climate change and human activity to unveil the process of global environmental evolution and to predict future development trends (Aguilar et al. 2012; Pouliot et al. 2009).

The remote sensing (RS) technology have been widely applied in ecological research (Cabello et al. 2012; Feng et al. 2010; Pettorelli et al. 2005; Xie et al. 2008). Moderate Resolution Imaging Spectroradiometer (MODIS) data have been widely used since the launch of Terra platform in December 1999. The Normalized Difference Vegetation Index (NDVI) product from MODIS have been widely applied for vegetation research (Eisfelder et al. 2012; Fensholt et al. 2012). In recent decades, many studies have used NDVI data to monitor and evaluate variations in vegetation over different spatial and temporal scales, including research into vegetation phenology and terrestrial carbon cycle (Azzali and Menenti 2000), the characteristics of different crop species (Jakubauskas et al. 2002), forest fires (Jia et al. 2004; Leblon et al. 2001), the impacts of human activities on vegetation dynamics and distribution (Possingham et al. 2016), and vegetation cover characteristics and its response to climate change (Fensholt et al. 2009; Ma and Frank 2006; Pelkey et al. 2003; Wen et al. 2017). However, these impacts were rarely considered in the greenness trend of vegetation in global karst area, so as the influence of natural process and human activities effects on vegetation change. The study could provide foundations for the predicting of vegetation growth trends, ecosystem evolution and environmental change in the global karst regions. What's more, due to the seasonal variations in solar radiation and vegetation growth, Seasonally Integrated Normalized Difference Vegetation Index (SINDVI) works better than NDVI in reflecting inter-annual mutability and integrative vegetation cover trends (Sun et al. 2010). In addition, SINDVI, defined as the sum of NDVI values (NDVI > 0.1) in all time phases for each pixel during the growing season, can effectively eliminate the impact of regions with bare and sparse vegetation (Hope et al. 2003; Stow et al. 2003). SINDVI has been widely applied in exploring the land use and vegetation change, such as in Ejin Oasis (Hu et al. 2015), and the effect of vegetation change on albedo (Li et al. 2018) and land surface temperature (Song et al. 2018). Based on previous research, we aimed to provide since the beginning of the 21th century information on the different vegetation in the global karst regions in this study. There were two main research objectives of the current study: (1) to investigate the overall trends of vegetation greenness and climate variables, applied Mann-Kendall to detect potential breaking points of SINDVI time series data, and (2) to analyzed changes in SINDVI and their relationships with climate factors and land cover change.

Datasets and Methods

Study area

Global karst regions, with a total area of 2.2×10^7 km^2 were chooses as the study area in this research (Fig. 1). The World Karst Map V3.0 was obtained from Geography and Environmental Science, University of Auckland (https://www.fos.auckland.ac.nz/our_research/karst/index.html). To improve the accuracy of boundary information for the karst areas, the World Karst Map V3.0 data were integrated with detailed karst data in each continent by Karst Scientific Data Center and is available from http://www.karstdata.cn. There is a prominent karst zone around the world from western China through the Middle East to the Mediterranean and along the coast of the western Atlantic. There are three major karst regions in the world: East Asia, the Mediterranean coast and eastern America. In specific, these include southwestern China, northern Vietnam, central and southern Europe, the central plateau of France, Ural in Russia, northeastern America, Cuba and Jamaica. According to climatic conditions, karst areas be divided into 4 categories: the glacial karst area, Eurasian plate karst area, North American plate karst area, and Gondwana continental karst area. Most karst regions have suffered from a series of ecosystem damages, including rocky desertification, soil erosion, vegetation degeneration, and productivity decline. In particular, Mexico, Middle East, Southeast Asia (Ford and Williams 2007), southwest China (Jiang et al. 2014) and Mediterranean basin (Yassoglou 2000) are the most ecologically fragile areas in the world (Kelly et al. 2011).

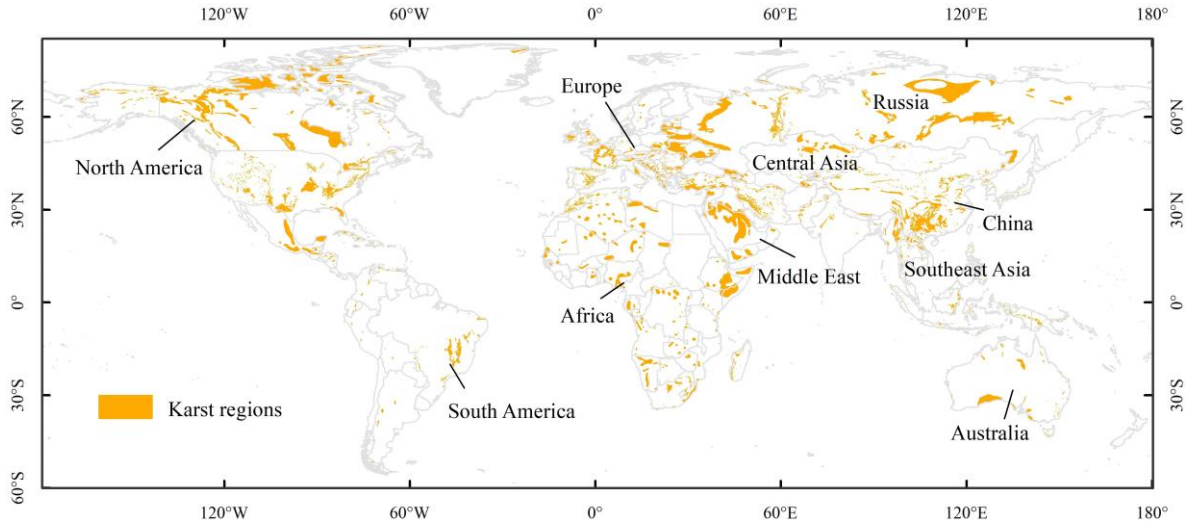

Fig. 1 Global distribution of karst regions

Datasets

Vegetation index data

This study selected the MODIS/Terra NDVI (collection 6) dataset, which was based on cloud-free composites images from 16 days with a spatial resolution of 1 km (Wen et al. 2017). The NDVI data were supplied as a Level 3 product projected onto a 0.05-degree (5600 m) Climate Modeling Grid (CMG) with monthly temporal resolution, provided by Land Processes Distributed Active Archive Center (LP DAAC), the NASA Earth Science Data and Information System project, available from (https://doi.org/10.5067/MODIS/MOD13C2.006).

SINDVI was defined as the sum of NDVI values greater than certain threshold (0.1 was selected in this study) in all time phases throughout the year of each pixel (Hope et al. 2003; Ma and Frank 2006; Stow et al. 2003), it was calculated by summing monthly NDVI values when NDVI > 0.1 for each pixel as bellow:

$$SINDVI = \sum_{i=0}^{i=12} NDVI_i \quad (NDVI > 0.1,\ i=1,2,\ldots,12) \tag{1}$$

where *i* represents the *i*th month.

Meteorological data

Meteorological parameters including air temperature and precipitation were obtained from GLDAS_NOAH025_M data, Goddard Earth Sciences Data and Information Services Center (https://disc.gsfc.nasa.gov/datasets/GLDAS_NOAH025_M_2.1/summary?keywords=GLDAS), which were processed in monthly 0.25-degree resolution. The GLDAS air temperature was instantaneous observation per 3 hours, which firstly generated into monthly temperature by averaging, and then generated to the scale of annual temperature was in this study. While the GLDAS precipitation was the sum of rain and snow amount per 3 hours, which was firstly calculated to monthly precipitation and then accumulated to annual. GLDAS-2.1 data were archived in machine independent and self-describing NetCDF format. MATLAB R2016b was used to convert data format and synthesize meteorological data to a yearly scale.

Land cover data

To monitorand quantify the land cover change over the full time period in global karst regions, the Terra and Aqua combined MODIS (MCD12C1, V 6.0) data product (https://doi.org/10.5067/MODIS/MCD12Q1.006) were used. Maps of the International Geosphere-Biosphere Programme (IGBP), University of Maryland (UMD), and Leaf Area Index (LAI) classifications schemes are provided at annual scale at 0.05 degree (5,600 meter) spatial resolution for the entire globe, the dataset is available from 2001 to 2019.

Methods

Reconstruct NDVI data

The Mean Value Iteration filter (MVI), a simple and effective method was used to reconstruct NDVI and reduce the noise caused by the atmosphere water vapor and clouds. The reconstruction process can also eliminate some NDVI outliers in the original image, improving the homogeneity of each land cover type and spatial uniformity of NDVI image (Ma and Veroustraete 2006). A high quality of NDVI time series was calculated as follows:

$$\Delta i = \left|NDVI_i - (NDVI_{i-1} + NDVI_{i+1})\right| / 2 \tag{2}$$

where *i* means the *i*th monthly NDVI. 10% of the multiyear NDVI average of each pixel was set at a threshold (ΔT), when Δi is greater than ΔT, NDVI will be replaced by $NDVI_i - (NDVI_{i-1} + NDVI_{i+1})/2$. Finally, when all Δi are less than ΔT the iteration ended.

Time series analyses

The monthly SINDVI, air temperature, and precipitation from 2001 to 2020 were processed to synthesize the annual data, therefore time series in each pixel had a length of 20 years. In order to estimate the inter-annual trends of SINDVI, meteorological parameters, and area for different land use types, we used an ordinary least squares method to calculate their slops and ranges in different karst regions (Hu et al. 2015; Li et al. 2018; Peng et al. 2018). The slopes, representing the change rates of each pixel from 2001 to 2020, were calculated as follows:

$$\text{Slope} = \frac{n \times \sum_{i=1}^{n}(i \times X_i) - \sum_{i=1}^{n} i \times \sum_{i=1}^{n} X_i}{n \times \sum_{i=1}^{n} i^2 - (\sum_{i=1}^{n} i)^2} \quad (3)$$

where n is the cumulative number of years in the monitoring period; i is the serial number of years and i=1, 2, … 20; and X_i is the SINDVI, air temperature, or precipitation in the ith year. Slopes > 0 indicates that variables are increasing in n years, while slopes < 0 means a downward trend. The more the slope values are near to 0, the much less changes are occurred in the trends (Jafary et al. 2018). To detect statistical significance of the variables trends in karst regions from 2001 to 2020, a Pearson correlation analysis was used and significance level was set to 0.05 ($P < 0.05$) in this study.

The range was used to assess the magnitude of the changes. The value calculated for each pixel indicates the change between 2001 and 2020.

$$\text{Range} = \text{Slope} \times (\text{n-1}) \quad (4)$$

where n is the length of study periods.

Mann-Kendall test

Mann-Kendall analysis is a trend estimation method of time series based on nonparametric rank (Kendall 1975; Mann 1945), which is suitable for elastic processing of outliers (Lanzante 2015). The sequential version of the Mann-Kendal rank statistics can be performed using the following steps:

a. Replace original values of the series x_i by their ranks y_i, arrange in ascending order.

b. The magnitudes of y_i (i=2, …, n) were compared with y_j (j=1,…,i-1). At each comparison, the number of cases $y_i > y_j$ was markede by r_i.

c. For the time series X, which containing n samples, a rank sequence (S_m) was first constructed as follows:

$$S_m = \sum_{i=1}^{m} r_i \ (m = 2, 3, \ldots, n) \quad (5)$$

where m is length of study periods; S_m is the sum of all individual S statistics (r_i) for all years

d. r_i is the cumulative number of the ith sample when $y_i > y_j$ and it was defined as follows:

$$r_i = \begin{Bmatrix} 1 & x_i > x_j \\ 0 & x_i \le x_j \end{Bmatrix} \quad (6)$$

e. Considering that the time series are independent and random, the statistical UF is defined as follows:

$$UF_m = \frac{[S_m - E(S_m)]}{\sqrt{\text{Var}(S_m)}} \ (m = 1,2,3,\ldots,n) \quad (7)$$

f. E (S*m*) is the mathematical probabilities; and Var (S*m*) is the variances. E (S*m*) and Var (S*m*) were calculated as follows:

$$E(S_m) = \frac{n(n\text{-}1)}{4} \quad (8)$$

$$Var(S_m) = \frac{n(n\text{-}1)(2n\text{+}5)}{72} \quad (9)$$

where n is the number of observations. A positive value of UF_m indicates an increasing trend, which is a series of positive statistics calculated by range x_1, x_2, x_3, … , x_n. Subsequently, calculating the inverted sequence of time series X (x_n, x_{n-1}, …, x_1) by repeating the above process, to obtain the reverse statistical sequence UB_m. If UB_m and UF_m intersect, their intersection may be a breakpoint ($P < 0.05$).

Correlation analysis

In order to explorethe relationship between SINDVI and meteorological parameters (air temperature and precipitation), Pearson's correlation coefficients (r) were calculated as follows:

$$r_{xy} = \frac{\sum_{i=1}^{n}(x_i\text{-}\bar{x})(y_i\text{-}\bar{y})}{\sqrt{\sum_{i=1}^{n}(x_i\text{-}\bar{x})^2}\sqrt{\sum_{n=1}^{n}(y_i\text{-}\bar{y})^2}} \quad (10)$$

where r_{xy} is the correlation coefficient between x and y, and the values range from -1 to 1; x_i and y_i are the values of the ith year; $\bar{x}$ and $\bar{y}$ are their averages for 20 years.

Partial correlations were conducted to assess the dominant factor of each pixel. When estimating the partial correlation between temperature and SINDVI, the influence of precipitation will be considered as a constant. For example, if the partial correlation coefficient between SINDVI and temperature was greater than the correlation coefficient between SINDVI and precipitation, it indicates that temperature had larger influence on SINDVI. The partial correlation coefficients were calculated as follows:

$$r_{yz\cdot x} = \frac{r_{yz}\text{-}r_{yx}r_{zx}}{\sqrt{(1\text{-}r_{yx}^2)(1\text{-}r_{zx}^2)}} \quad (11)$$

where $r_{yz\cdot x}$ is the partial correlation coefficient between y and z without consideration the influence of x; and r_{xy} and r_{xz} are the simple correlation coefficient between x and y. For each pixel, the dominant by comparing the partial coefficient between NDVI and temperature or precipitation. Different significance levels were also set for difference confidence interval (Extremely significant, $P < 0.01$; very significant, $P < 0.05$; significant, $P < 0.1$; not significant, $0.1 < P < 1$).

Results

Spatiotemporal variation in SINDVI

Temporally, SINDVI showed an obvious increase trend during the period of 2001 – 2020 in karst regions, with an average of 3.99. While, there was large spatial heterogeneity (**Fig. 2a**), with the largest average SINDVI values appeared in China and Europe.

There were remarkable and widespread increment of SINDVI in the global karst areas during the research period (**Fig. 2**). In general, approximately 72.35% of the pixels showed upward trends. Meanwhile, there were also spatial differences between various regions. Especial the obvious disparity of the increasing trends appeared in tropical regions, subtropical humid regions and temperate regions. Notably, the increasing trend of the SINDVI in China was the most obvious, which increased 0.836 from 2001 to 2020 (**Fig. 2b**). In contrast, the decreasing trends of SINDVI mainly distributed in arid areas, such as -0.020 in Central Asia and -0.006 in South America respectively.

. The positive trends of SINDVI at low latitudes in the Northern Hemisphere were generally weaker than in middle and higher latitudes (**Fig. 2b**). In additional, SINDVI in the Northern Hemisphere growth 0.28, while there was no significant trend in the Southern Hemisphere.

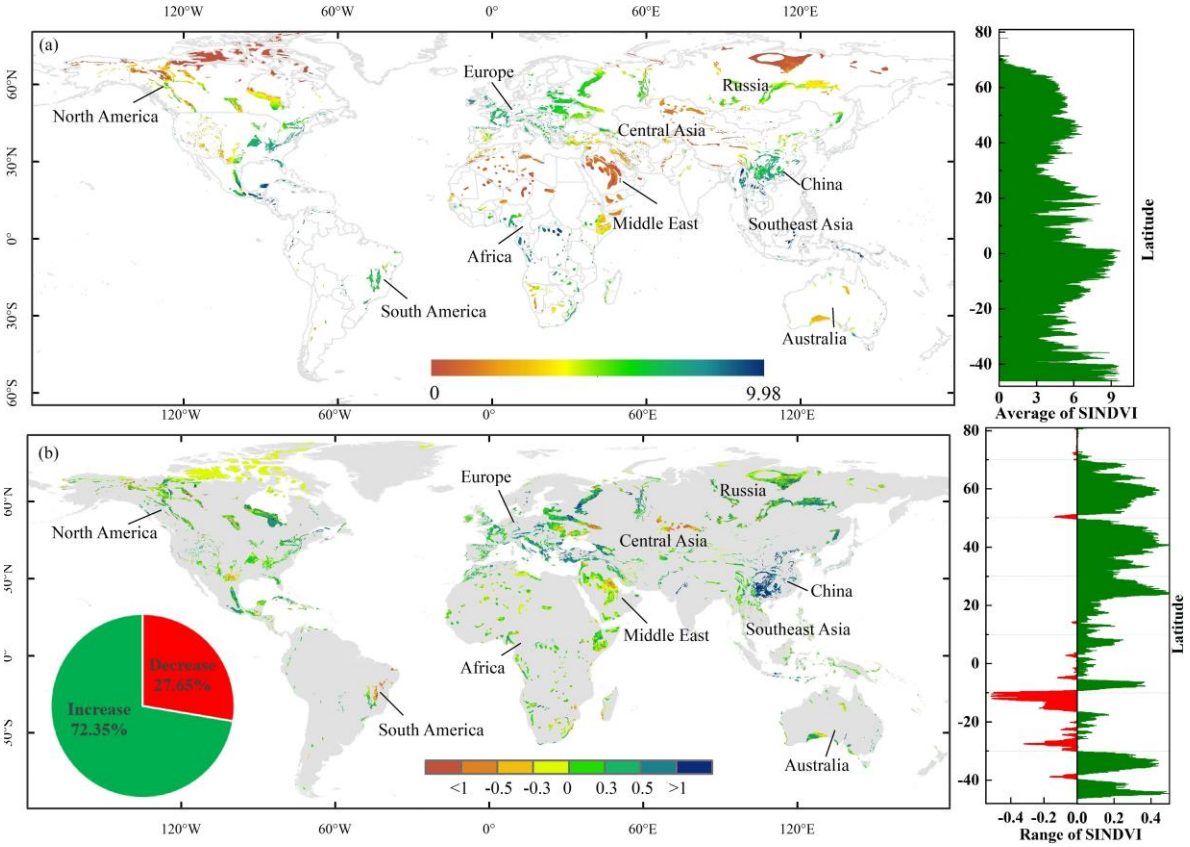

Fig. 2 Average (a) and change range (b) of the SINDVI during the period of 2001-2020 in the global karst areas. Pie chart at the lower left corner (b) shows the percentages of increasing and decreasing SINDVI pixels. Bar charts in the right show the latitudinal distribution of averages (a) and ranges (b) of SINDVI.

From 2001 to 2020, SINDVI in the global karst regions showed an increasing trend with large volatility (**Fig. 3b**) (slope = 0.011/a, $P < 0.01$). The sequential version of the Mann-Kendall tests was conducted to detect the breakpoints (**Fig. 3a**). The forward (UF) and backward (UB) statistics sequence curves intersected near the year of 2012, indicating that there was a significant change in SINDVI around 2012. Before the breakpoint, SINDVI exhibited a stronger positive trend with a rate of 0.011/a ($P < 0.05$). However, after the breakpoint, the SINDVI exhibited a relatively weaker positive trend with a rate of 0.009/a ($P < 0.05$). In order to determine the patterns of inter-annual trends, we calculated the trends of both before the breakpoint (BBP) and after the breakpoint (ABP) for all regions and classified them into four categories (**Fig. 4**): increased in BBP but decreased in ABP, decreased in BBP but increase in ABP, upward trends in both BBP and ABP, and downward trends in both

BBP and ABP. The results showed that the NINDVI in Australia, Middle East, Russia and South America showed climbed in BBP but decreased trends in ABP. China, North America, Europe, Africa and Southeast Asia showed sustained increasing trends from 2001 to 2020 at the rate of 0.034/a, 0.028/a, 0.011/a, 0.006/a and 0.005/a in BBP respectively. After that, with the exception of North America, the growth trends of the other three regions were stronger after the turning points. Central Asia showed a continuous downward trend, with the breakpoints in 2009, and the decreasing trends in ABP were weaker than those in BBP.

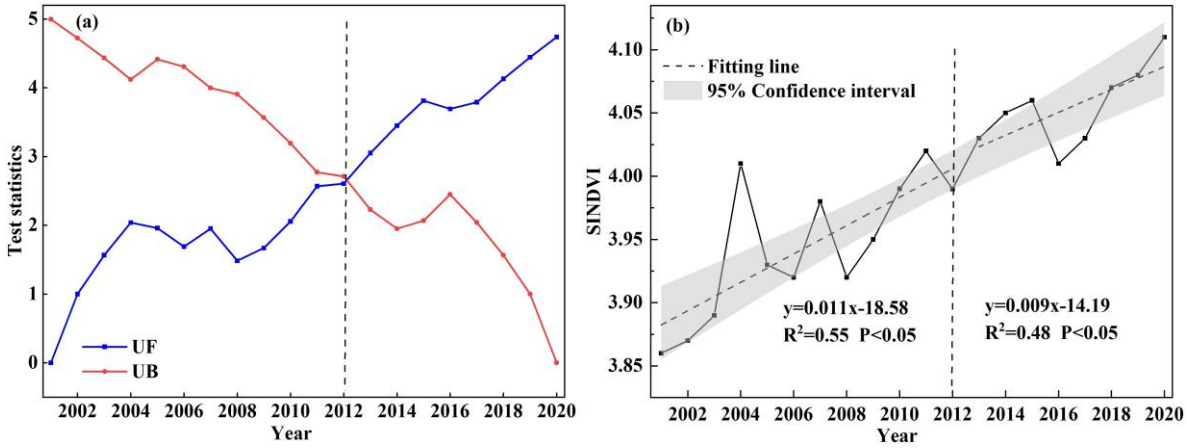

Fig. 3 Abrupt changes (a) and inter-annual variations (b) of SINDVI from 2001 to 2020. UF is the positive sequence of time series and UB is the negative sequence. UF and UB larger than 0 indicates increasing trends. The point where two curves intersect is the breakpoint (P < 0.05).

Table 1 Change rates of SINDVI overall trend, BBP trend and ABP trend in global karst regions.

Karst regions	BP year	Trend slope		
		Allover	BBP	ABP
Africa	2007	0.003	0.006	0.041
Australia	2012	0.006	0.022	-0.004
China	2012	0.044	0.034	0.039
Central Asia	2009	-0.020	-0.039	-0.012
Europe	2012	0.024	0.011	0.024
Middle East	2012	0.011	0.004	-0.001
North America	2009	0.011	0.028	0.011
Russia	2011	0.004	0.029	-0.031
South America	2006	-0.006	0.012	-0.009
Southeast Asia	2011	0.011	0.005	0.018

*: BP, BBP and ABP represent breakpoint, before the breakpoint and after the breakpoint, respectively.

Relationship between SINDVI and meteorological factors

Fig. 4 illustrated the spatial patterns of the trend in precipitation and temperature in global karst areas during 2001 to 2020. The annual average temperature showed an increasing trend of 0.06 °C/a (P < 0.05) (Fig. 4a). Spatially, all the karst regions experienced air temperature warming trends, particularly in Africa

and Middle East where the magnitude of the temperature trend exceeds 2 ℃ during research period. Conversely, precipitation experienced slightly decreased at the rate of -0.36 mm/a (P > 0.05) (**Fig. 4b**), only China and Southeast Asia have increasing trends. The maximum of temperature and precipitation appeared in 2010, which trends were in good agreement with long-term trends in precipitation in previous study of Adler et al. (2017).

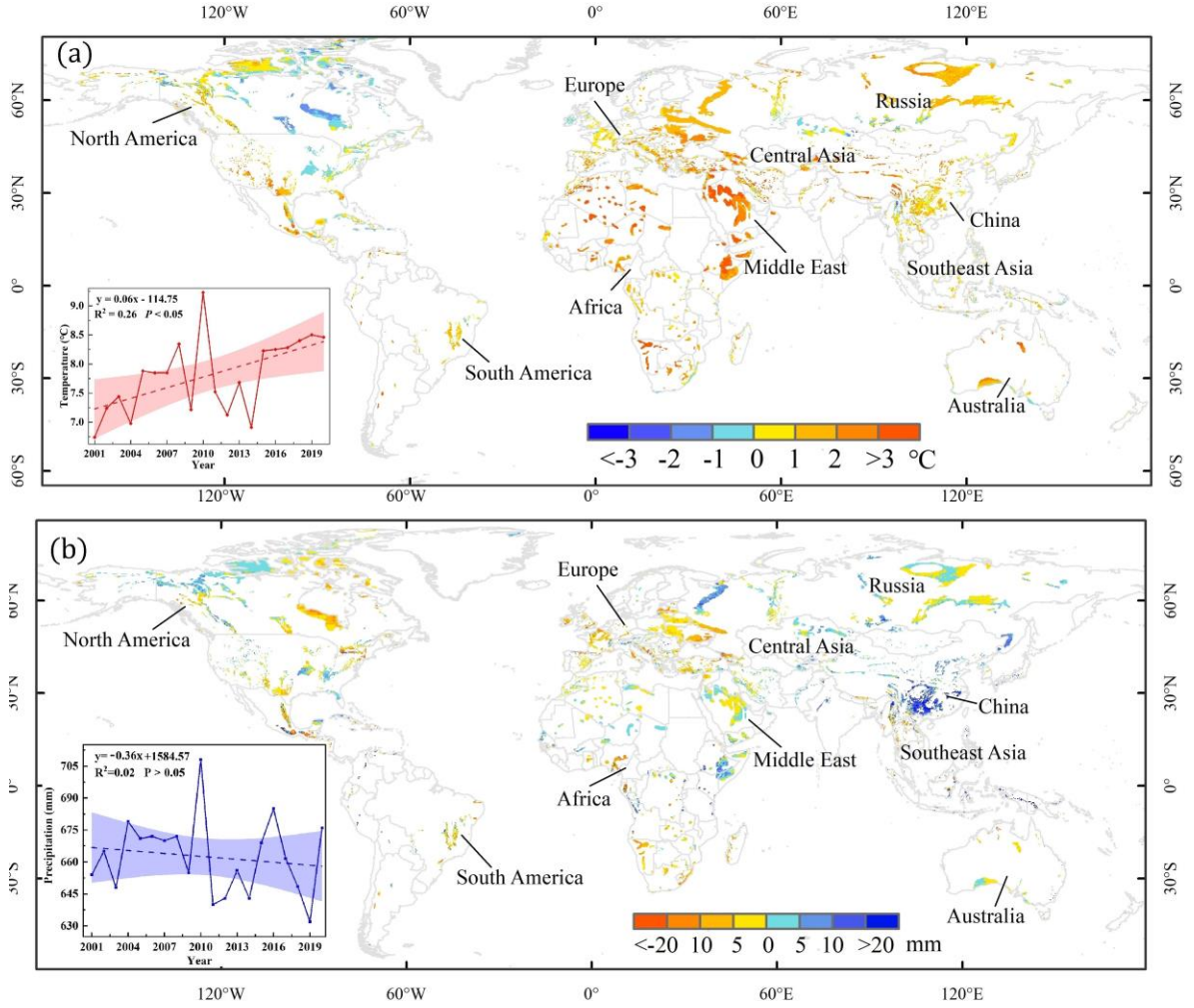

Fig.4 Spatial distribution of change range in (a) temperature and (b) precipitation. Line chart in lower left corner illustrated the inter-annual variations in air temperature and precipitation in global karst regions from 2001 to 2020.

278 **Table 2**. Overall changes of the SINDVI, air temperature and precipitation in global karst regions during the period of 2001-
279 2020.

Karst regions	SINDVI	Temperature (℃)	Precipitation (mm)
Africa	0.057	2.27	-3.87
Australia	0.114	1.52	-40.37
Central Asia	-0.380	0.50	49.30
China	0.836	1.40	188.32
Europe	0.456	1.46	-49.56
Middle East	0.209	2.46	-21.09
North America	0.209	0.27	-21.50
Russia	0.076	1.25	6.12
South America	-0.114	1.14	-19.94
Southeast Asia	0.209	0.75	220.47

280 In order to determine the spatial correlation between SINDVI and precipitation or air temperature, correlation
281 coefficients were calculated for each pixels (**Fig. 5**). About 21.12% of SINDVI pixels was affected by precipi-
282 tation ($P < 0.05$) in global karst regions. (**Fig. 5a**). Correlation coefficients greater than 0.5 mainly occurred in
283 Middle East peninsula, Mexico, Southwest China, Southern Australia and Southern Africa (**Fig. 5c**). Approxi-
284 mately15.22% pixels indicated that temperature have significant influenced on the variation of SINDVI (**Fig.**
285 **5b**), with *r* values larger than 0.5 were mainly distributed in Central Eurasia, Eastern Mediterranean, Eastern
286 and Northwest Canada, Southwestern China and Eastern United States (**Fig. 5d**).

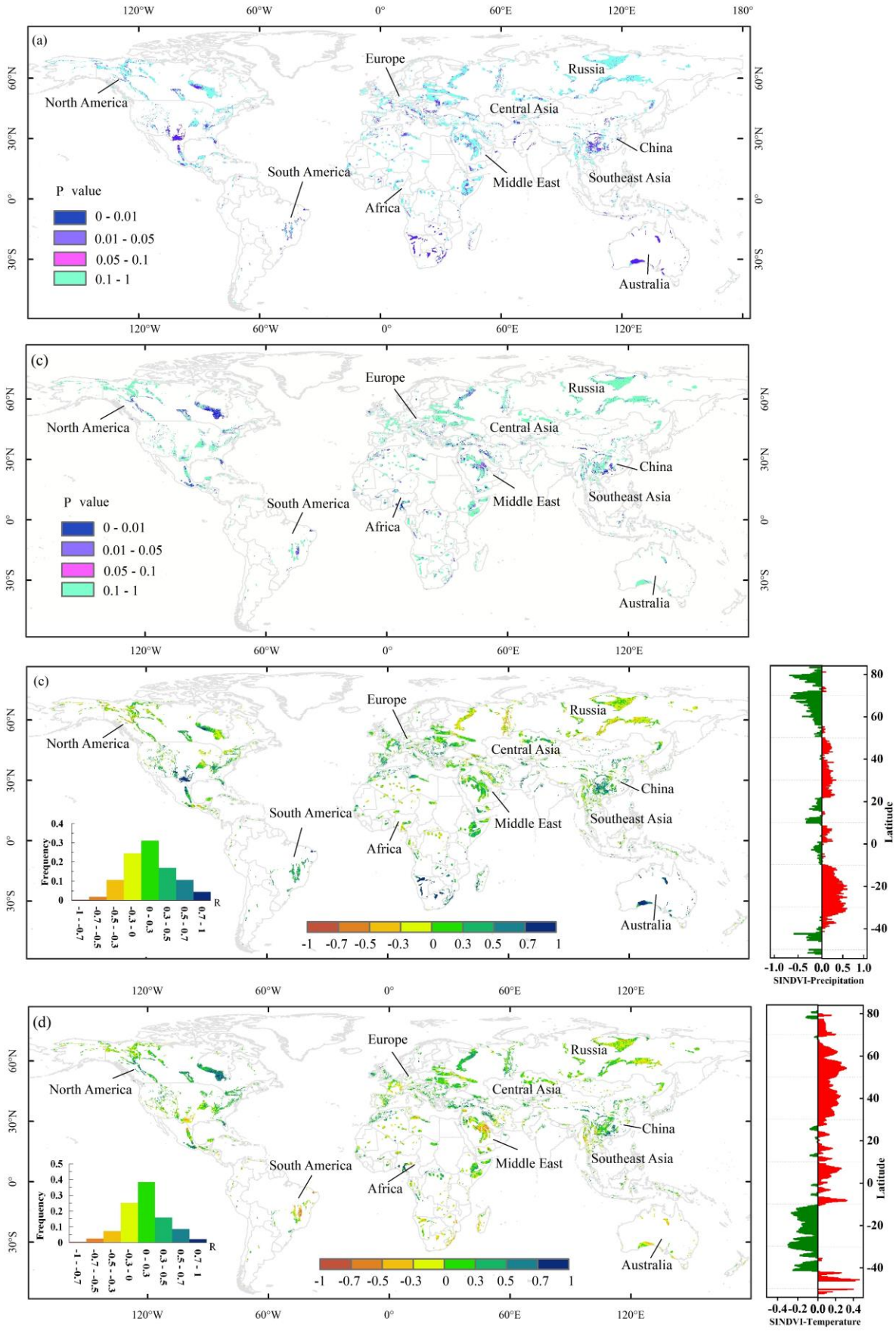

Fig. 5 Spatial significance levels of correlation (a) between SINDVI and precipitation, (b) between SINDVI and temperature from 2001 to 2020 in global karst areas. (c) The correlation coefficients between SINDVI and precipitation, and (d) between

SINDVI and temperature. Non-vegetation regions were removed. Histogram in the left is the frequency distribution of correlation coefficients of the pixel count.

The partial correlation coefficient was calculated for each pixel to determine the main factor of SINDVI change (**Fig. 6**), wherein only 21.06% of the areas are significance ($P < 0.05$). The karst regions of several different regions have analyzed below.

In the arid regions in the Southern Hemisphere, including Australia and South Africa, SINDVI dynamic were synergistic with precipitation change (**Fig. 6**). In near the equator, where the precipitation is abundant throughout the year, temperature seems to play a powerful role in the fluctuation of SINDVI.

In the high latitude areas of the Northern Hemisphere, temperature acted as the dominant factor affecting the SINDVI. All of the rising temperature, stronger photosynthesis and longer growth season, facilitated the plant growth vigorously and then promoted SINDVI.

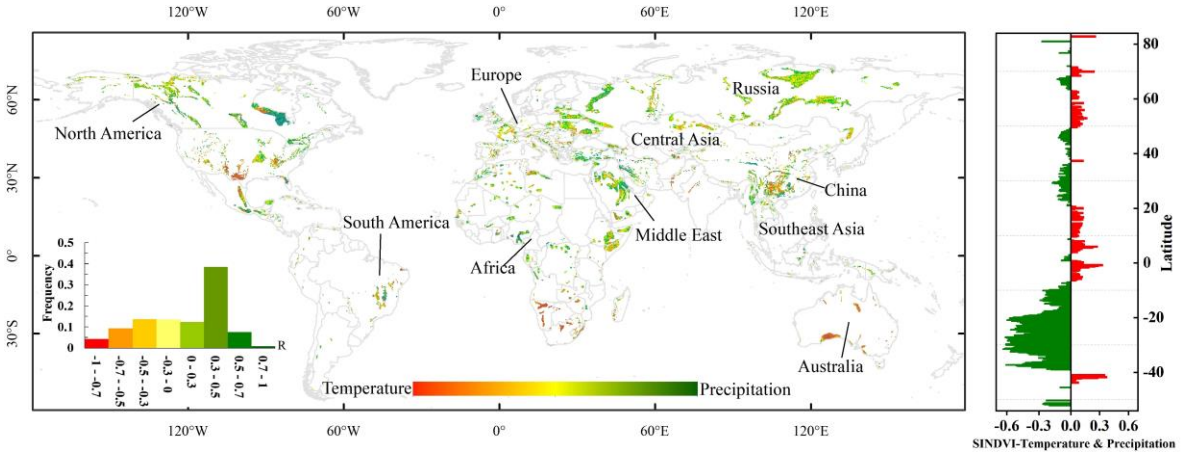

Fig. 6 Partial correlation coefficient of SINDVI with temperature and precipitation in global karst areas. The green color represents the area where precipitation is the main factor of SINDVI change; while the red color represents the area where temperature is the dominant factor. Histogram in the lower left corner is the frequency distribution of correlation coefficients.

Trend of land cover change in karst regions

Since we interested in changes in type of vegetation cover, and take into account only five land uses in the karst regions: cropland, forest, shrub land, grassland and bare land the dominant types in global karst regions were grassland, and forest. Between 2001 and 2019, grassland area has increased from 438.986×10^4 km^2 to 443.810×10^4 km^2 with a rate of 0.2868×10^4 km^2/a, cropland area has a slightly increasing at the rate of 0.0936×10^4 km^2/a. In contrast, the shrub land, forest and bare land exhibited decreasing trends with rates of -0.1103×10^4 km^2/a, -0.1598×10^4 km^2/a and -0.0771×10^4 km^2/a, respectively (**Fig. 7**).

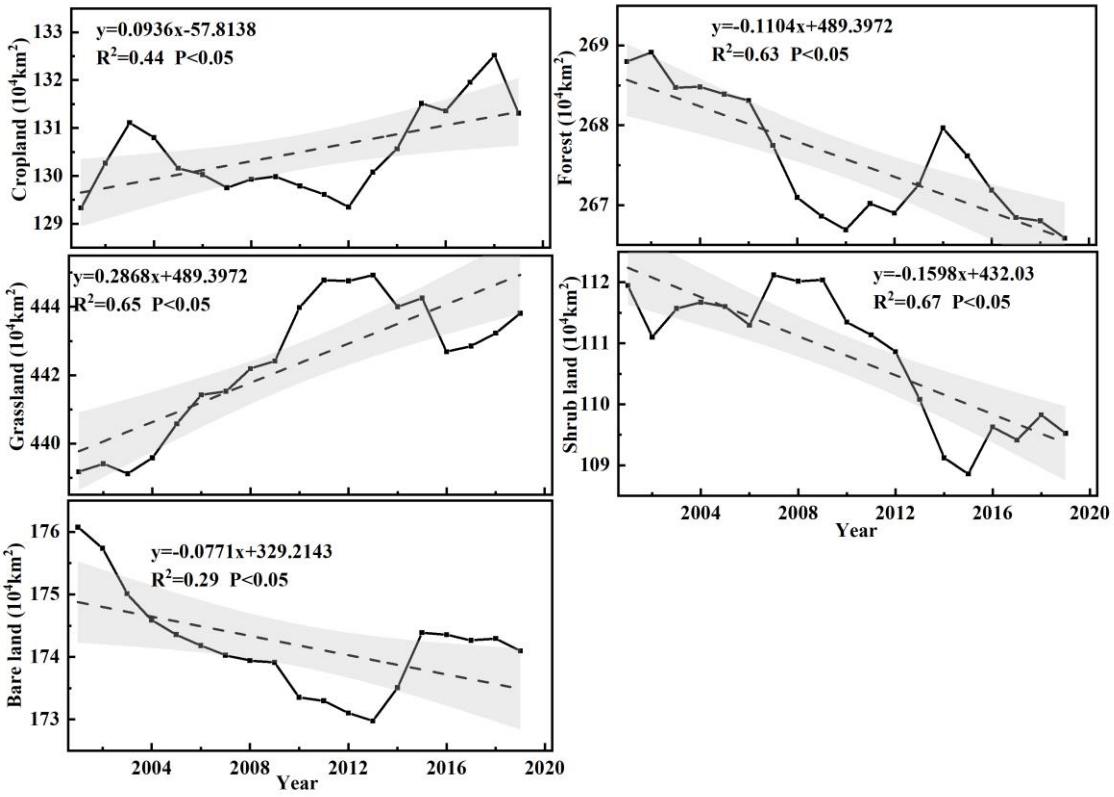

Fig. 7 Temporal changes of land cover types in global karst regions from 2001 to 2019.

At the regional scale, the various land cover types undergo different changes at different regions, and a detailed statistical analysis of the five main land cover types were performed for ten karst regions (**Fig. 8**). The cropland area reduced in Europe, China, Africa and Southeast Asia. In terms of forest, with exception of Russia, Africa, North America, South America and Middle East, all other regions showed increasing trends. In additional, most regions experienced the disappearing of shrub land excepted three regions (Central Asia, Australia and Southeast Asia).For grasslands, besides five regions (Central Asia, Australia, Europe, Middle East and Southeast Asia), all other regions showed upward trends. Regarding bare land, China, Africa and North America remarkably dropped, conversely, while Middle East has positive trend, and other regions have no visible changes.

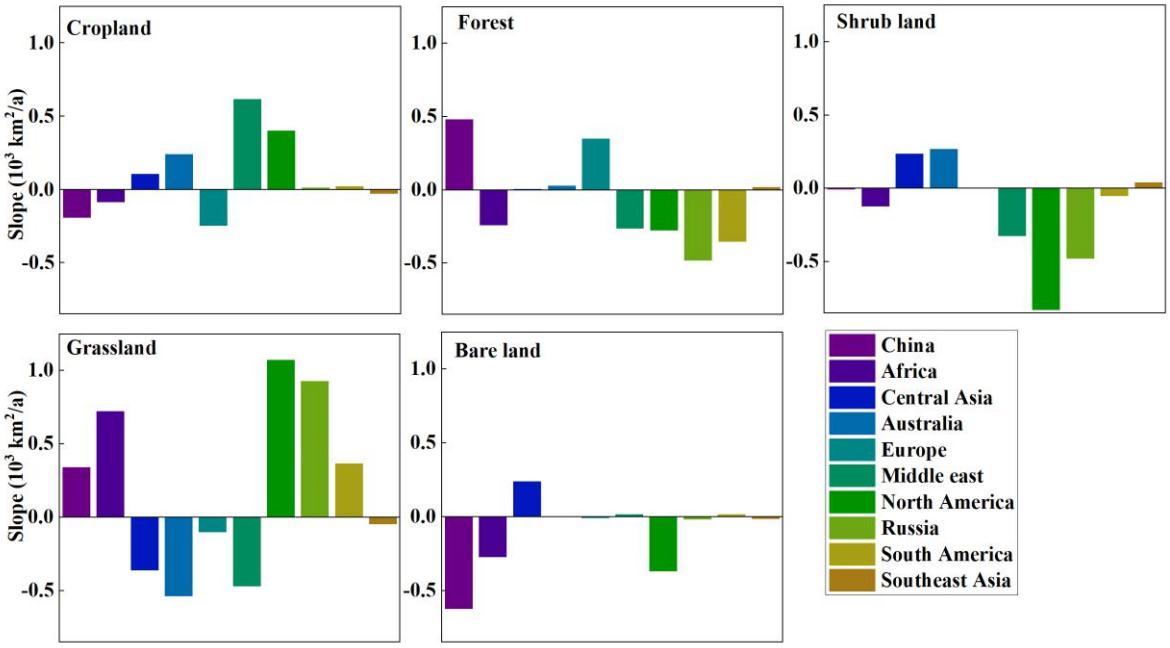

Fig. 8 Change rates of the land cover types in different karst regions from 2001 to 2019

Discussions

Our results indicate that the spatio-temporal variations of SINDVI over the global karst regions show a greening trend during 2001-2020 (slope = 0.011/a, P < 0.01), which is consistent with previous study (Zhang et al., 2017, Piao et al. 2020). There are two distinct periods with growing trends in SINDVI, in the first period (**Fig. 3**), SINDVI has significantly increased from 2001 to 2012 (slope = 0.011/a, P < 0.01), and then relatively weaker grown from 2012 to 2020 (slope = 0.009/a, P < 0.01). Changes in the latter period is largely contributed by the browning vegetation which occurred in Australia and Middle East after 2012, and Russia after 2011 respectively. Which offset the greening trend before 2012 in other karst regions, this finding also consistent with previous reports (Long et al. 2018, Piao et al. 2020).

This study also indicates that climate change is the most important factor influencing vegetation dynamics in karst regions (**Fig. 5**),which is in a good agreement with previous results (Piao et al. 2014).During the research period, two meteorological factors (air temperature and precipitation) had significantly positive relationships with the inter-annual SINDVI variation in the global karst regions, indicating that the increase of temperature and precipitation could promote the growth of vegetation.

Despite the positive correlation between temperature and SINDVI in most karst areas of the Northern Hemisphere, including China, Europe and North America, the significant negative correlation also appeared in most dry areas and the middle-latitude areas, such as South Africa, Southern Australia, Middle East (**Fig. 5d**). In the dry areas, the persistent warming and decreasing of precipitation can seriously aggravate the water deficit and evapotranspiration loss, bringing heavy damage to plant growth (Zhou et al. 2015). Because of obvious spatiotemporal differences, this study chosen several regions with obvious variation of SINDVI to explore the related in global karst areas. Increasing trends in the SINDVI

Vegetation in the karst areas of China has increased in the last decade (**Fig.2b**). The relationship between SINDVI and temperature was closer than that between SINDVI and precipitation (**Fig. 6**). This might be related

to the location of Southwestern China, which is the subtropical monsoon climate zone, with adequate precipitation. Therefore, small changes of precipitation may not cause seriously change on vegetation growth (Lai et al. 2020; Hou et al. 2015; Zhao et al. 2017). In addition, the dual hydrological structures of surface and underground in karst region in Southwest China lead to drainage of precipitation through leakage and runoff (Tong et al. 2016), indicating the precipitation has limited effect of vegetation growth. As for the reason behind the greening in this area, on the one hand, governments have taken some effective measures (e.g., relocation and ecological migration) to reduce land abandonment and land degradation caused by the outflow of rural population (Chen et al. 2019). On the other hand, ecosystem restoration projects (for example, the Grain to Green Project, the Karst Rocky Desertification Restoration Project, and the Natural Forest Protection Project) have been implemented (Mueller et al. 2014; Tong et al. 2018; Zhang 2008) are considered an important factor in turning green, especially in China since 2008.

The similar political decisions appeared in Europe, the afforestation and forest management have accelerated the growth of vegetation (Naudts et al. 2016), causing the dramatic increase in the forest area of 0.3485×10^3 km^2/a (**Fig. 8**) and contributing to the upward trend in the SINDVI. Furthermore, the rising temperature (Range = 1.46 ℃) might have promoted the growth of vegetation, which may explain the greening trend. Previous study indicated that the positive effect of meteorological parameters change in the northern high latitudes were attributed to nitrogen deposition and CO_2 concentration in the boreal forests, other factors including enhanced photosynthesis and prolonged growing seasons (LeBauer and Treseder 2008; Liu et al. 2015; Menzel et al. 2006; Xu et al. 2013). In central and northeastern America, the increasing temperature was the dominant factor affected the SINDVI (**Fig. 5d**), this upward trend was contributed to vegetation propagation caused by global warming (Zhu et al. 2016). Moreover, agricultural fertilization and irrigation would also have a significant impact on the trend of SINDVI dynamics (Neigh et al. 2008) In contrast, the effect of precipitation was stronger than that of temperature in southern North America (**Fig. 6**). **Fig. 3** shows that the BP of the inter-annual variation in SINDVI occurred in 2012, the SINDVI showed an increasing trend with a slope of 0.028/a before breaking point (BBP); while, the upward trend was relatively slight (slope = 0.011/a) after the breakpoint (ABP). The extreme climate and the cool winters in 2009/2010, 2010/2011, and 2013/2014 in North America led to anomalous vegetation growth (Yu and Zhang 2015).

For arid and semi-arid areas, the land use type is mainly savanna and desert, although the trend in vegetation cover is similar to that of global level, their extents of changes are differently. Precipitation is characterized by regular seasonal drought and large inter-annual fluctuation. Due to the non-irrigated crops and natural ecosystems mainly depend on soil moisture produced by snow melt in spring and seasonal rainfall (Baldocchi et al. 2004; Zaitchik et al. 2007), there is large inter-annual fluctuation in the vegetation coverage (**Fig. 4**). The drought episodes that struck the Middle Eastern countries in 2007-2009 were the worst drought events to impact the region in more than 60 years (Villa et al. 2014). What's more, both the dominant impact of the lower precipitation and the climbed temperature (**Table. 2**) in this period provide the sufficient conditions of extreme drought in this area. Nonetheless, a fact that a faster recovery of cropland in intensive agricultural areas, these greening trends were due to farming in the North Iraq and Turkey for which groundwater and desalinated seawater were used (Rousta et al. 2020). In the low latitudes, except for temperature and precipitation, solar radiation is also a limiting factor (Nemani et al. 2003). In Southeast Asia the NDVI product may include some inaccuracies. We applied the Maximum Value Composite (MVC) method to reduce the outliers of data, but the selected maximum value is not always the nadir value that tends to overestimate NDVI values (Huete et al.

2002). Moreover, the NDVI value saturates easily under high vegetation coverage and cannot sensitively monitor the changes in vegetation growth (Wang et al. 2003). These issues associated with NDVI also influence the accuracy of the correlations.

In order to evaluate the temporal evolution of low vegetation areas when NDVI < 0.1 (**Fig. 9**), we found that Middle East, Arctic tundra and the Sahara have greening trends, while central Asia shew a browning trend. These results, at least in part, are in agreement with previous studies (Berner et al. 2020, Piao et al. 2020 Rousta et al. 2020)

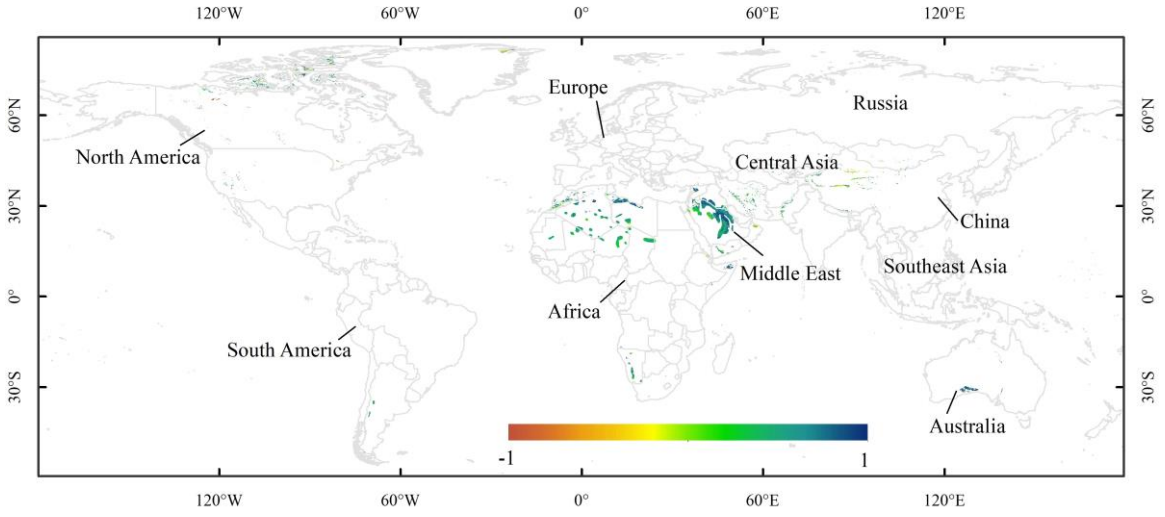

Fig. 9 Spatial distribution of change range of NDVI < 0.1.

Decrease trends in SINDVI

Located in the hinterlands of the Eurasian continent, Central Asia is one of the driest areas in the world (Cihlar et al. 1997) with low vegetation coverage. Most area is desert in this region besides Tajikistan and Kyrgyzstan which are predominantly mountainous. The variation of SINDVI indicates that vegetation degradation mainly occurred in northern Kazakhstan, southern Tajikistan and southwestern Kyrgyzstan. The spatial distribution of temperature from 2001 to 2020 showed a significance warming trend (**Fig. 4**), although the slightly increasing trend in precipitation, sufficient sunlight and solar energy resources in these domains are abundant than other places, resulting in annual precipitation less than annual evapotranspiration; thus, Excessive evapotranspiration is the hinge process of soil moisture loss and leads to the shallow roots of desert plants to withered (Li et al. 2015; Yuan et al. 2017). In the drought periods, moisture insufficiency inhibited the growth of vegetation and reduced photosynthesis of plants (Stocker et al. 2019; Zhang et al. 2012).

This study found the sharply decreasing trend of the forest cover of Russia, Africa, North America, South America and Middle East (**Fig. 8**), mainly caused by fire, diseases or even over-logging (for example, large areas tree mortality in North America owning to plant disease and insect pests (Yang, et al. 2017); Middle East and South America experienced a widespread deforestation and fire (Aparna et al. 2020; Qin et al. 2017)). This study also found that the increment of grassland and cropland areas in these regions make contribution to the positive trend of SINDVI, which is consistent with the findings that cropland land increase in some regions and that the increase in vegetation greenness occurred in regions of intensive agricultural activities (Hansen et al. 2014; Lamchin et al. 2020).

In the Northern Hemisphere, vegetation growth was mainly affected by temperature, while precipitation was the dominant factor to the change of vegetation greenness in the Southern Hemisphere. The karst areas of South America, which are mainly in the east of Brazil. According to **Table 2**, SINDVI here showed a downward trend, and the vegetation coverage in this region did not couple with temperature and precipitation. This lack of correlation is attributed to heavy human intervention. Under pressure from human society, land use change is increasingly threatening tropical rainforest area (Dirzo and Raven 2003). The quick transformation of forests into agricultural, timber production and other uses has produced a vast and human dominated landscape, which will bring immeasurable destruction to the rainforest (Gardner et al. 2009, Hansen et al. 2014). However, some studies have shown that the occurrence of extreme weather in recent years has aggravated the natural disasters, such as the severe droughts occurred in Brazil in 2007 (Cunha et al. 2019).

This study aimed to observe the impact of meteorological parameters change and human environmental protection policies on vegetation dynamic from 2001 to 2020. Our results indicate that the karst ecosystem is particularly vulnerable to the alternation of seasonal drought and flood. Especially in the 21th century, under intensive anthropogenic activities and climate changes (extreme weather events), fragile karst terrains have been facing the threat of serious ecosystem degradation. This study assesses the important issues including anthropogenic disturbance and climate change in karst area on global or regional scales. In particular, we have elaborated the impact of climate change in Southwest China, human activities were the dominate factor of vegetation greening, while in 2009/2010, there was a downward trend in SINDVI due to a period of extreme drought (Li et al. 2019; Zhao et al. 2017). Many previous studies also have confirmed that abnormal cyclone in the western North Pacific during an El Niño period resulted in a severe reduction in precipitation in Southwest China in the autumn of 2009 (Zhang et al. 2013). Climate change has caused large variations in seasonal and annual precipitation and temperature, both locally and globally (Fernández et al. 2014). Especially in the recent decades, drought occurred with longer durations, greater intensities and more frequently, with the serious impact on karst ecosystem (Trenberth et al. 2014; Williams et al. 2015). Deep rooting plant access to bedrock water storage and groundwater is an importance feature to plant survival in drought environments (Ding et al. 2020, Wang et al. 2019). For example, the effects of droughts have been widely reported in the karst areas in the United States (Ganguli and Ganguly 2016), Europe (Spinoni et al. 2017) and central equatorial Africa (Hua et al. 2016). A better knowledge of the dynamics of vegetation greenness and it responses to extremely climate is an essential process in understanding current situations and project future changes. The current study is mainly about the global karst vegetation change, with focuses on several fragile karst regions. The results provide scientific evidence for the protection of fragile karst ecosystem, while detailed studies in each karst area are still needed.

Conclusions

In summary, this study assessed spatiotemporal variations in vegetation cover by estimating global SINDVI trends for karst region. On a global karst scale, inter-annual SINDVI of the karst regions from 2001 to 2020 exhibited an upward trend by 0.011/a. Temperature and precipitation had prominent effect on inter-annual changes in SINDVI with large spatiotemporal heterogeneities. In dry areas such as Central Asia, persistent warming coupled with decreasing precipitation caused serious water deficit and great evapotranspiration loss, thus affected the growth of vegetation. However, in some middle and high latitude areas, warming temperature was considered to be the main reason for greening trends, such as in northern Eurasia and northern North America. In addition to studying climate factors (temperature and precipitation), this study assessed anthropogenic

activities (e.g., Ecological Engineering, the Grain to Green Project) also have significant impact on the variations in SINDVI.

Acknowledgments In this study, we archived multi-resource datasets from different data centers. The data include the MODIS NDVI, GLDAS-2.1data, land cover data and population density data. They were provided by USGS, ESA and SEDAC. The authors express their gratitude for the data sharing of above datasets.

Author Contributions Conceptualization, Jing Huang and Mingguo Ma; Data curation, Xuguang Tang; Formal analysis, Jing Huang, Yuqing Huang and Xuguang Tang; Funding acquisition, Mingguo Ma; Methodology, Jing Huang, Zhongxi Ge and BinfeiHao; Resources, Mingguo Ma; Software, Peiyu Lai, BinfeiHao and Zengjing Song; Validation, Zhan Shi; Writing – original draft, Jing Huang and Zhongxi Ge; Writing – review & editing, Jing Huang, Yuqing Huang, Peiyu Lai, Hong Yang and Mingguo Ma.

Funding This work was jointly supported by supported by the National Natural Science Foundation of China projects (grant numbers: 41830648 and 41771453), the Fundamental Research Funds for the Central Universities of China (Grant No. XDJK2015C007), National Key Technology R&D Program of China (grant number: 2016YFC0500106).

Conflicts of Interest The authors declare no conflict of interest.

References

Adler, R.F., Gu, G., Sapiano, M. et al. (2017) Global Precipitation: Means, Variations and Trends During the Satellite Era (1979–2014). Surv Geophys 38: 679–699. https://doi.org/10.1007/s10712-017-9416-4.

Aguilar C, Zinnert JC, Polo MJ, Young DR (2012) NDVI as an indicator for changes in water availability to woody vegetation. Ecol Indic 23: 290-300. https://doi.org/10.1016/j.ecolind.2012.04.008.

Aparna R. Phalke, Mutlu Özdoğan, Prasad S. Thenkabail, Tyler Erickson, Noel Gorelick, Kamini Yadav, Russell G. Congalton (2020) Mapping croplands of Europe, Middle East, Russia, and Central Asia using Landsat, Random Forest, and Google Earth Engine. ISPRS J PHOTOGRAMM 167: 104-122. https://doi.org/10.1016/j.isprsjprs.2020.06.022.

Azzali S, Menenti M (2000) Mapping vegetation-soil-climate complexes in southern Africa using temporal Fourier analysis of NOAA-AVHRR NDVI data. Int J Remote Sens 21: 973-996. https://doi.org/10.1080/014311600210380.

Baldocchi DD, Xu LK, Kiang N (2004) How plant functional-type, weather, seasonal drought, and soil physicalproperties alter water and energy fluxes of an oak-grass savanna and an annual grassland. Agric For Meteor 123. https://doi.org/10.1016/j.agrformet.2003.11.006.

488 Begue A, Vintrou E, Ruelland D, Claden M, Dessay N (2011) Can a 25-year trend in Soudano-Sahelian
489 vegetation dynamics be interpreted in terms of land use change? A remote sensing approach. Glob
490 Environ Chang 21: 413-420. https://doi.org/10.1016/j.gloenvcha.2011.02.002.
491 Berner, LT, Massey, R, Jantz, P et al. (2020) Summer warming explains widespread but not uniform greening
492 in the Arctic tundra biome. Nat Commun 11: 4621. https://doi.org/10.1038/s41467-020-18479-5.
493 Cabello J, Fernández N, Alcaraz-Segura D, Oyonarte C, Piñeiro G, Altesor A, Delibes M, Paruelo JM (2012)
494 The ecosystem functioning dimension in conservation: insights from remote sensing. Biodivers
495 Conserv 21: 3287-3305. https://doi.org/10.1007/s10531-012-0370-7.
496 Cao J, Jiang Z, Yuan D, Xia R, Zhang C (2017) The progress in the study of the karst dynamic system and
497 global changes in the past 30 years. Geol in China 44: 874-900.
498 Chen C, Park TJ, Wang XH, Piao SL, Xu B, Chaturvedi RK, Fuchs R, Brovkin V, Ciais P, Fensholt R,
499 Tømmervik H, Bala G, Zhu ZC, Nemani RR, Myneni RB (2019) China and India lead in greening of
500 the world through land-use management. Nat Sustain 2: 122-129. https://doi.org/10.1038/s41893-019-
501 0220-7.
502 Chen X, Pan W (2010) Relationships among phenological growing season, time-integrated normalized
503 difference vegetation index and climate forcing in the temperate region of eastern China. Int J Climatol
504 22: 1781-1792. https://doi.org/10.1002/joc.823.
505 Cihlar J, Ly H, Li ZQ, Jing C, Pokrant H, Huang FT (1997) Multitemporal, multichannel AVHRR data sets for
506 land biosphere studies—Artifacts and corrections. Remote Sens Environ 60: 35-57.
507 https://doi.org/10.1016/s0034-4257(96)00137-x.
508 Cunha APMA, Zeri M, Leal KD, Costa L, Cuartas LA, Marengo JA, Tomasella J, Vieira RM, Barbosa AA
509 (2019) Extreme Drought Events over Brazil from 2011 to 2019. Atmos 10.
510 https://doi.org/10.3390/atmos10110642.
511 De Jong R, Schaepman ME, Furrer R, De Bruin S, Verburg PH (2013) Spatial Relationship Between
512 Climatologies and Changes in Global Vegetation Activity. Glob Chang Biol 19: 1953-1964.
513 https://doi.org/10.1111/gcb.12193.
514 Dirzo R, Raven PH (2003) Global state of biodiversity and loss. Annu Rev EnvironResour 28: 137-167.

Ding YL, Nie YP, Chen HS, Wang KL, Querejeta JI (2021) Water uptake depth is coordinated with leaf water potential, water-use efficiency and drought vulnerability in karst vegetation. New Phytol 229: 1339-1353. https://doi.org/10.1111/nph.16971.

Eisfelder C, Kuenzer C, Dech S (2012) Derivation of biomass information for semi-arid areas using remote-sensing data. Int J Remote Sens 33: 2937-2984. https://doi.org/10.1080/01431161.2011.620034.

Falkowski P, Scholes RJ, Boyle E, Canadell J, Canfield D, Elser J, Gruber N, Hibbard K, H?Gberg P, Linder S (2000) The global carbon cycle: a test of our knowledge of earth as a system. Science 290: 291-296. https://doi.org/10.1126/science.290.5490.291.

Feng X, Fu B, Yang X, Lü Y (2010) Remote sensing of ecosystem services: An opportunity for spatially explicit assessment. Chinese Geogra Sci 20: 522-535. https://doi.org/10.1007/s11769-010-0428-y.

Fensholt R, Proud SR, Simon R (2012) Evaluation of Earth Observation based global long term vegetation trends — Comparing GIMMS and MODIS global NDVI time series. Remote Sens Environ 119: 131-147. https://doi.org/10.1016/j.rse.2011.12.015.

Fensholt R, Rasmussen K, Nielsen TT, Mbow C (2009) Evaluation of earth observation based long term vegetation trends — Intercomparing NDVI time series trend analysis consistency of Sahel from AVHRR GIMMS, Terra MODIS and SPOT VGT data. Remote Sens Environ 113: 1886-1898. https://doi.org/10.1016/j.rse.2009.04.004.

Fernández ME, Gyenge JE, Varela S, De Urquiza M (2014) Effects of the time of drought occurrence within the growing season on growth and survival of Pinus ponderosa seedlings. Trees 28: 745–756. https://doi.org//10.1007/s00468-014-0986-1.

Florinsky IV, Kuryakova GA (1996) Influence of topography on some vegetation cover properties. Catena 27: 123-141. https://doi.org/10.1016/0341-8162(96)00005-7.

Ford D, Williams P (2007) Karst Hydrogeology and Geomorphology. John Wiley & Sons Ltd, England.

Ganguli P, Ganguly AR (2016) Space-time trends in U.S. meteorological droughts. JHydrol: Reg Stud 8: 235–259. https://doi.org/10.1016/j.ejrh.2016.09.004.

Gardner TA, Barlow J, Chazdon R, Ewers RM, Harvey CA (2009) Prospects for tropical forest biodiversity in a human-modified world. Ecol Lett 12: 561–582. https://doi.org/10.1111/j.1461-0248.2009.01294.x.

542 Hansen M, Potapov P, Margono B, Stehman S, Turubanova S, Tyukavina A (2014) Response to comment on
543 "High-resolution global maps of 21st-century forest cover change". Science 342: 850-853.
544 https://doi.org/10.1126/science.1248817.
545 Hope AS, Boynton WL, Stow DA, Douglas DC (2003) Interannual growth dynamics of vegetation in the
546 Kuparuk River watershed, Alaska based on the Normalized Difference Vegetation Index. Int J Remote
547 Sens 24: 3413-3425. https://doi.org/10.1080/0143116021000021170.
548 Hou WJ, Gao JB, Wu SH, Dai E (2015) Interannual Variations in Growing-Season NDVI and Its Correlation
549 with Climate Variables in the Southwestern Karst Region of China. Remote Sens 7: 11105-11124.
550 https://doi.org/10.3390/rs70911105.
551 Hu XL, Lu L, Li X, Wang JH, Lu XG (2015) Ejin Oasis Land Use and Vegetation Change between 2000
552 and2011: The Role of the Ecological Water Diversion Project. Energies 8: 7040-7057.
553 https://doi.org/10.3390/en8077040.
554 Hua W, Zhou L, Chen H, Nicholson SE, Jiang Y (2016) Possible causes of the Central Equatorial African long-
555 term drought. Environ Res Lett 11: 124-138. https://doi.org/10.1088/1748-9326/11/12/124002.
556 Huang MT, Piao SL, Ciais P, Peñuelas J, Wang XH, Keenan TF, Peng SS, Berry JA, Wang K (2019) Air
557 temperature optima of vegetation productivity across global biomes. Nat Ecol Evol 3: 772-779.
558 https://doi.org/10.1038/s41559-019-0838-x.
559 Huang YQ, Zhao P, Zhang ZF, Li XK, He CX, Zhang RQ (2000) Transpiration of Cyclobalanopsis glauca (syn.
560 Quercus glauca) stand measured by sap-flow method in a karst rocky terrain during dry season. Ecol
561 Res 24: 791-801. https://doi.org/10.1007/s11284-008-0553-6.
562 Huete A, Didan K, Miura T, Rodriguez EP, Gao X, Ferreira LG (2002) Overview of the radiometric and
563 biophysical performance of the MODIS vegetation indices. Remote Sens Environ 83: 195-213.
564 https://doi.org/10.1016/S0034-4257(02)00096-2.
565 Jafary P, Sarab AA, Tehrani NA (2018) Ecosystem Health Assessment Using a Fuzzy Spatial Decision Support
566 System in Taleghan Watershed Before and After Dam Construction. Environ Process 5: 807-831.
567 https://doi.org/10.1007/s40710-018-0341-4.
568 Jakubauskas ME, Legates DR, Kastens JH (2002) Crop identification using harmonic analysis of time-series
569 AVHRR NDVI data. Comput Electron Agric 37: 127-139. https://doi.org/10.1016/S0168-
570 1699(02)00116-3.

Jia GJ, Epstein HE, Walker DA (2004) Controls over intra-seasonal dynamics of AVHRR NDVI for the Arctic tundra in northern Alaska. Int J Remote Sens 25: 1547-1564. https://doi.org/10.1080/0143116021000023925.

Jiang L, Jiapaer G, Bao A, Guo H, Ndayisaba F (2017) Vegetation dynamics and responses to climate change and human activities in Central Asia. Sci Total Environ 599-600: 967-980.

Jiang ZC, Lian YQ, Qin XQ (2014) Rocky desertification in Southwest China: Impacts, causes, and restoration. Earth-Sci Rev 132: 1-12. https://doi.org/10.1016/j.earscirev.2014.01.005.

Kelly M, Tuxen KA, Stralberg D (2011) Mapping changes to vegetation pattern in a restoring wetland: Finding pattern metrics that are consistent across spatial scale and time. Ecol Indic 11: 263-273. https://doi.org/10.1016/j.ecolind.2010.05.003.

Kendall M (1975) Rank correlation methods. London: Charles Griffin.

Lai P, Zhang M, Ge Z, Hao B, Han X (2020) Responses of Seasonal Indicators to Extreme Droughts in Southwest China. Remote Sensing 12: 818. https://doi.org/10.3390/rs12050818.

Lanzante JR (1996) Resistant, Robust and Nonparametric Techniques for the Analysis of Climate Data: Theory and Examples, Including Applications to Historical Radiosonde Station Data. Int J Climatol 16: 1197-1226. https://dx.doi.org/10.1002/(SICI)1097-0088(199611)16:11<1197::AID-JOC89>3.0.CO;2-L.

Lamchin M, Wang SW, Lim CH, Ochir A, Pavel U, Gebru BM, Choi Y, Jeon SW, Lee WK (2020), Understanding global spatio-temporal trends and the relationship between vegetation greenness and climate factors by land cover during 1982 - 2014. Glob Ecol Conserv 24: e01299. https://doi.org/10.1016/j.gecco.2020.e01299.

LeBauer DS, Treseder KK (2008) Nitrogen limitation of net primary productivityin terrestrial ecosystems is globally distributed. Ecology 89: 371-379. https://doi.org/10.1890/06-2057.1.

Leblon B, Alexander B, Chen J, White S (2001) Monitoring fire danger of northern boreal forests with NOAA-AVHRR NDVI images. Int J Remote Sens 22: 2839-2846. https://doi.org/10.1080/01431160121183.

Li QP, Ma MG, Wu XD, Hong Y (2018) Snow cover and vegetation-induced decrease in global albedo from 2002 to 2016. J Geophys Res Atmos: 124-138. https://doi.org/10.1002/2017JD027010.

Li X, Li Y, Chen A, Gao M, Slette I, Piao SL (2019) The impact of the 2009/2010 drought on vegetation growth and terrestrial carbon balance in Southwest China. Agric For Meteorol 269: 239-248. https://doi.org/10.1016/j.agrformet.2019.01.036.

600 Li Z, Chen YN, Li WH, Deng HJ, G F (2015) Potential impacts of climate change on vegetation dynamics in
601 Central Asia. J Geophys Res Atmos 120: 12345-12356. https://doi.org/10.1002/2015JD023618.
602 Liu C, Yun Z, Chao S, Hou H, Li X (2012) Effect of Farm Manure on Dissolution of Underlying Carbonate
603 Rocks and Atmospheric CO_2 Source/Sink. https://doi.org/10.1007/978-3-642-27682-8_15.
604 Liu Y, Li Y, S.C L, Motesharrei S (2015) Spatial and Temporal Patterns of Global NDVI Trends: Correlations
605 with Climate and Human Factors. Remote Sens 7: 13233-13250. https://doi.org/10.3390/rs71013233.
606 Liu ZJ, Liu YS, Li YR (2018) Anthropogenic contributions dominate trends of vegetation cover change over
607 the farming-pastoral ecotone of northern China. Ecol Indic 95: 370-318.
608 https://doi.org/10.1016/j.ecolind.2018.07.063.
609 Long XJ, Guan HD, Sinclair R, Batelaan O et al. (2018) Response of vegetation cover to climate variability in
610 protected and grazed arid rangelands of South Australia. J Arid Environ 161: 64-71.
611 https://doi.org/10.1016/j.jaridenv.2018.10.001.
612 Ma Mg, Veroustraete F (2006) Reconstructing pathfinder AVHRR land NDVI time-series data for the
613 Northwest of China. Advances in Space Research 37: 835-840. https://doi.10.1016/j.asr.2005.08.037.
614 Ma Mg, Frank V (2006) Interannual variability of vegetation cover in the Chinese Heihe River Basin and its
615 relation to meteorological parameters. Int J Remote Sens 27: 3473-3486.
616 https://doi.org/10.1080/01431160600593031.
617 Mann HB (1945) Nonparametric Tests Against Trend. Econ Soc 13: 245-259.
618 Martínez B, Gilabert MA (2009) Vegetation dynamics from NDVI time series analysis using the wavelet
619 transform. Remote Sens Environ 113: 1823-1842. https://doi.org/10.1016/j.rse.2009.04.016.
620 Menzel A, Sparks TH, Estrella N, Koch E, Aasa A, Ahas R (2006) European phenological response to climate
621 change matches the warming pattern. Glo Change Bio 12: 1969−1976.https:/doi.org/10.1111/j.1365-
622 2486.2006.01193.x.
623 Mueller T, Dressler G, Tucker CJ, Pinzon JE, Leimgruber P, Dubayah RO, Hurtt GC, Böhning-Gaese K, Fagan
624 WF (2014) Human Land-Use Practices Lead to Global Long-Term Increases in Photosynthetic
625 Capacity. Remote Sensing 6: 5717-5731. https://doi.org/10.3390/rs6065717.
626 Naudts K, Chen YY, McGrath MJ, Ryder J, Valade A, Otto J (2016) Europe's forest management did not
627 mitigate climate warming. Science 315: 597-600. https://doi.org/10.1126/science.aad7270.

628 Ndayisaba F, Hao G, Bao A, Hui G, Karamage F, Kayiranga A (2016) Understanding the Spatial Temporal
629 Vegetation Dynamics in Rwanda. Remote Sens 8: 129-146. https://doi.org/10.1002/joc.823.
630 Neigh CSR, Tucker CJ, Townshend JRG (2008) North American vegetation dynamics observed with multi-
631 resolution satellite data. Remote Sens Environ 112: 1749-1772.
632 https://doi.org/10.1016/j.rse.2007.08.018.
633 Nemani RR, Keeling CD, Hirofumi H, Jolly WM, Piper SC, Tucker CJ, Myneni RB, Running SW (2003)
634 Climate-driven increases in global terrestrial net primary production from 1982 to 1999. Science 300:
635 1560-1563. https://dx.doi.org/10.1126/science.1082750.
636 Pelkey NW, Stoner CJ, Caro TM (2003) Assessing habitat protection regimes in Tanzania using AVHRR NDVI
637 composites: Comparisons at different spatial and temporal scales. Int J Remote Sens 24: 2533-2558.
638 https://doi.org/10.1080/01431160210155929.
639 Peng J, Ma J, Liu Q, Liu Y, Hu Y, Li Y, Yue Y (2018) Spatial-temporal change of land surface temperature
640 across 285 cities in China: An urban-rural contrast perspective. Sci Total Environ 635: 487-497.
641 https://doi.org/10.1016/j.scitotenv.2018.04.105.
642 Peters GP, Andrew RM, Boden T, Canadell JG, Ciais P, Quéré CL, Marland G, Raupach MR, Wilson C (2012)
643 The challenge to keep global warming below 2 °C. Nat Clim Chang 3: 4-6.
644 https://doi.org/10.1038/nclimate1783.
645 Pettorelli N, Vik JO, Mysterud A, Gaillard JM, Tucker CJ, Stenseth NC (2005) Using the satellite-derived
646 NDVI to assess ecological responses to environmental change. Trends Ecol 20: 503-510.
647 https://doi.org/10.1016/j.tree.2005.05.011.Piao SL, Nan H, Huntingford C, Ciais P, Friedlingstein P,
648 Sitch S, Peng S,, Canadell JG, Cong N (2014) Evidence for a weakening relationship between
649 interannual temperature variability and northern vegetation activity. Nat Commun 5: 5018-5022.
650 https://doi.org/10.1038/ncomms6018.
651 Piao SL, Yin GD, Tan JG, Cheng L, Huang MT, Li Y (2015) Detection and attribution of vegetation greening
652 trend in China over the last 30 years. Glob Change Biol 21: 1601-1609.
653 https://doi.org/10.1111/gcb.12795.
654 Piao, SL., Wang, XY., Park, T et al. (2020) Characteristics, drivers and feedbacks of global greening. Nat Rev
655 Earth Environ 1: 14–27. https://doi.org/10.1038/s43017-019-0001-x.Possingham HP, Laurance WF,
656 Wood P, Fekete BM, Levy MA, Watson JEM (2016) Sixteen years of change in the global terrestrial

657 human footprint and implications for biodiversity conservation. Nat Commun 7: 1-11.
658 https://doi.org/10.1038/ncomms12558.
659 Pouliot D, Latifovic R, Olthof I (2009) Trends in vegetation NDVI from 1km AVHRR data over Canada for
660 the period 1985-2006. Int J Remote Sens 30: 149-168. https://doi.org/10.1080/01431160802302090.
661 Qin YW, Xiao XM, Dong JW, Zhou YT, Wang J, Doughty RB., Chen Y, Zou ZH, Moore B (2017), Annual
662 dynamics of forest areas in South America during 2007–2010 at 50-m spatial resolution: Remote Sens
663 Environ 201: 73-87.
664 Rousta I, Olafsson H, Zhang H, Moniruzzaman M, Krzyszczak J, Baranowski P (2020) Anthropogenic Factors
665 Affecting the Vegetation Dynamics in the Arid Middle East. Preprints: 2020100208
666 https://doi.org/10.20944/preprints202010.0208.v2.
667 Seddon AWR, Maciasfauria M, Long PR, Benz D, Willis KJ (2016) Sensitivity of global terrestrial ecosystems
668 to climate variability. Nature 531: 229-232. https://doi.org/10.1038/nature16986.
669 Song ZJ, Li RH, Qiu RH, Liu SY, Tan C, Li QP (2018) Global Land Surface Temperature Influenced by
670 Vegetation Cover and PM2.5 from 2001 to 2016. Remote Sens 10: 2034-2052.
671 https://doi.org/10.3390/rs10122034.
672 Spinoni J, Naumann G, Vogt JV (2017) Pan-European seasonal trends and recent changes of drought frequency
673 and severity. Global Planet Change 148: 113–130. https://doi.org/10.1016/j.gloplacha.2016.11.013.
674 Stocker BD, Zscheischler J, Keenan TF, Prentice IC (2019) Drought impacts on terrestrial primary production
675 underestimated by satellitemonitoring. Nat Geosci 12. https://doi.org/10.1038/s41561-019-0318-6.
676 Stow D, Daeschner S, Hope A, Douglas D, Petersen A, Myneni R, Zhou L, Oechel W (2003) Variability of the
677 seasonally integrated normalized difference vegetationindex across the north slope of Alaska in the
678 1990s. Int J Remote Sens 24: 1111–1117. https://doi.org/10.1080/0143116021000021170.
679 Sun YL, Yang Y, Zhang L, Wang ZL (2015) The relative roles of climate variations and human activities in
680 vegetation change in North China. Phys Chem Earth 87-88: 67-78.
681 https://doi.org/10.1016/j.pce.2015.09.017.
682 Sun ZD, Chang NB, Opp C, Hennig T (2010) Evaluation of ecological restoration through vegetation patterns
683 in the lower TarimRiver, China with MODIS NDVI data. Ecol Inform 6: 156-163.
684 https://doi.org/10.1016/j.ecoinf.2010.10.002.

685 Tong XW, Wang KL, Brandt M, Yue YM, Liao C, Fensholt R (2016) Assessing Future Vegetation Trends and
686 Restoration Prospects in the Karst Regions of Southwest China. Remote Sens 8: 357.
687 https://doi.org/10.3390/rs8050357.
688 Tong XW, Brandt M, Yue YM, Horion S, Wang Kl, Keersmaecker WD, Tian F, Schurgers G, Xiao Xm, Luo
689 Yq (2018) Increased vegetation growth and carbon stock in China karst via ecological engineering.
690 Nat Sustainability 1: 44-50. https://doi.org/10.1038/s41893-017-0004-x.
691 Tong XW, Wang KL, Yue YM, Brandt M, Liu B, Zhang CH, Liao CJ, Fensholt R (2017) Quantifying the
692 effectiveness of ecological restoration projects on long-term vegetationdynamics in the karst regions
693 of Southwest China. Earth ObsGeoinf 54: 105-113. https://doi.org/10.1016/j.jag.2016.09.013.
694 Trenberth KE, Dai A, Schrier GVD, Jones PD, Barichivich J, Briffa KR, Sheffield J (2014) Global warming
695 and changes in drought. Nat Clim Change 4: 17-22. https://doi.org/10.1038/nclimate2067.
696 Vermote EF, Saleous EL, Nazmi Z, Christopher O (2002) Atmospheric correction of MODIS data in the visible
697 to middle infrared: first results. Remote Sens Environ 83: 97-111. https://doi.org/10.1016/S0034-
698 4257(02)00089-5.
699 Villa P, Boschetti M, Scozzari A, Vignudelli S (2014) Analysis of vegetation dynamics in middle east area
700 during 2002–2013 in relation to the 2007–2009 drought episode. IEEE GeosciRemote Sens Symp.
701 Wang ZX, Liu C, Huete A (2003) From AVHRR-NDVI to MODIS-EVI: Advances in vegetation index
702 research. Acta Ecol Sini 23: 979-987. https://doi.org/10.1023/A:1022289509702.
703 Wang KL, Yue YM, Brandt M, Tong XW (2019) Karst ecosystem observation and assessment at local and
704 regional scales. Inter Carto Inter GIS 25:43-47. http://doi.org/10.35595/2414-9179-2019-2-25-43-47.
705 Wen ZF, Wu SJ, Chen JL, Lü MQ (2017) NDVI indicated long-term interannual changes in vegetation activities
706 and their responses to climatic and anthropogenic factors in the Three Gorges Reservoir Region. Sci
707 Total Environ 574: 947-959. http://doi.org/10.1016/j.scitotenv.2016.09.049.
708 Williams AP, Seager R, Abatzoglou JT, Cook BI, Smerdon JE, Cook ER (2015) Contribution of anthropogenic
709 warming to California drought during 2012–2014. Geophys Res Lett 42: 6819–6828.
710 https://doi.org/10.1002/2015GL064924.
711 Xie YC, Sha Zy, Yu M (2008) Remote sensing imagery in vegetation mapping: a review. J Plant Ecol 1: 19-23.
712 https://doi.org/10.1093/jpe/rtm005.

713 Xu L, Myneni RB, Chapin FS, Callaghan TV, Pinzon JE (2013) Temperature and vegetation seasonality
714 diminishment over northern lands. Nat Clim Chang 3: 581-586. https://doi.org/10.1038/nclimate1836.
715 Yassoglou N (2000) History of desertification in the European Mediterranean. Pp. 9-15. In: Enne, G., D'Angelo,
716 M., Zanolla, C. (Eds.), Indicators for Assessing Desertification in the Mediterranean. Proceedings of
717 the International Seminar held in Porto Torres, Italy, 18-20 September, 1998. University of Sassari
718 Nucleo Ricerca Desertificazion, Sassari, Italy.
719 Yang J, Pan SF, Dangal S, Zhang B, Wang SY, Tian HQ (2017), Continental-scale quantification of post-fire
720 vegetation greenness recovery in temperate and boreal North America, Remote Sens Environ:
721 199:277-290. https://doi.org/10.1016/j.rse.2017.07.022.
722 Yu B, Zhang XB (2015) A physical analysis of the severe 2013/2014 cold winter in North America. J Geophys
723 Res Atmos 120: 10149-10165. https://doi.org/10.1002/2015jd023116.
724 Yuan DX (1993) Environmental change and human impact on karst in south China, in Williams, P., ed., Karst
725 terrains: environmental change and human impact. Catena Supplement 25.
726 Yuan DX (2000) Aspects on the new round land and resources survey in karst rock desertification areas of south
727 China. Carsologica Sinica 2: 2-7.
728 Yuan, XL, Wang, WF, Cui, JJ, Meng, F, Kurban, A, & De Maeyer, P (2017). Vegetation changes and land
729 surface feedbacks drive shifts in local temperatures over Central Asia. Scientific Reports, 7(1).
730 https://doi.org/10.1038/s41598-017-03432-2.
731 Yue YM, Zhang B, Wang KL, Zhang MY (2010) Spectral indices for estimating ecological indicators of karst
732 rocky desertification. Int J Remote Sens 31: 2115-2122. https://doi.org/10.1080/01431160903382892.
733 Zaitchik BF, Evans JP, Geerken RA (2007) Climate and vegetation in the Middle East: Interannual variability
734 and drought feedbacks. J Clim 20: 3924-3941. https://doi.org/10.1175/JCLI4223.1.
735 Zhang J (2008) Planning for comprehensive desertification control in Karst area of Guangxi Zhuang
736 Autonomous Region. Prat Sci 25: 93-102.
737 Zhang L, Xiao J, Li J, Wang K, Lei L, Guo H (2012) The 2010 spring drought reduced primary productivity in
738 southwestern China. Environ Res Lett 7: 045706. https://doi.org/10.1088/1748-9326/7/4/045706.
739 Zhang W, Jin F, Zhan J, Li Q, Ren H (2013) The possible influence of anonconventional El Niño on the severe
740 autumn drought of 2009 in southwest China. J Clim 26: 8392–8405. https://doi.org/10.1175/JCLI-D-
741 12-00851.1.Zhao S, Cong D, He K, Yang H, Qin Z (2017) Spatial-Temporal Variation of Drought in

China from 1982 to 2010 Based on a modified Temperature Vegetation Drought Index (mTVDI). Sci Rep 7: 17473. https://doi.org/10.1038/s41598-017-17810-3.

Zhou Y, Li Z, Fensholt R, Wang K, Vitkovskaya I, Feng T (2015) Climate Contributions to Vegetation Variations in Central Asian Drylands: Pre- and Post-USSR Collapse. Remote Sens 7: 2449-2470. https://doi.org/10.3390/rs70302449.

Zhu ZC, Piao SL, Myneni RB, Huang MT, Ning Z (2016) Greening of the Earth and its drivers. Nat Clim Chang 6: 791-795. https://doi.org/10.1038/nclimate3004.